Electronic Supplementary Material (ESI) for Catalysis Science & Technology.

Fluorinated phosphonium ionic liquid boosting the N_2-adsorbing ability of TiO_2 for efficient photocatalytic NH_3 synthesis

Xiang-Jiao Gong, Ben Chong, Meng-Yang Xia, He Li, Hong-Hui Ou*, Gui-Dong Yang*

XJTU-Oxford Joint International Research Laboratory of Catalysis, School of Chemical Engineering and Technology, Xi'an Jiaotong University, Xi'an, Shaanxi 710049, China

Corresponding author:
E-mail address: ouhonghui@xjtu.edu.cn; guidongyang@xjtu.edu.cn

1. Material and methods

1.1. Chemicals and materials

The reagents tetra-n-butyl titanate ($Ti(OBu)_4$•(TBOT), 99%), hydrofluoric acid solution (HF, 40wt%), NaOH (99%), ethanol (99%), sodium borohydride ($NaBH_4$, 98%), methanol (CH_3OH, 99%), and hydrochloric acid solution (HCl, 36~38 wt%) were purchased from Aladdin. Tetrabutylphosphonium hexafluorophosphate ($[P_{4,4,4,4}][PF_6]$, $C_{16}H_{36}F_6P_2$, 99%) were purchased from Shanghai Cheng Jie Chemical. The ultrapure water was obtained from water purification system (OSJ-UP). All the chemical reagents were used as received without further purification.

1.2. Synthesis of TiO_2 nanosheets

According to a previously reported procedure for the synthesis of TiO_2 nanosheets,[1] 3 mL of hydrofluoric acid solution was dropped into 25 mL of $Ti(OBu)_4$•(TBOT) under stirring for 2 h until the mixture changed into a gel. The gel was transferred into a dried Teflon autoclave (50 mL) and then the hydrothermal process was carried out at 180 °C

for 36 h. After cooling, the powder was separated by high-speed centrifugation and washed with ethanol and ultrapure water several times. At last, the powder was dispersed in 0.1 M NaOH aqueous solution and stirred for 8 h at room temperature. After high-speed centrifugation, the power was washed with ethanol and ultrapure water several times and then dried at 80 °C for 6 h.

1.3. Synthesis of protonated TiO_{2-x} nanosheets

A typical procedure after facile adjustments was used to get protonated TiO_{2-x} nanosheets. 100 mg of the above obtained TiO_2 power and 50 mg of $NaBH_4$ were replaced at both ends of the crucible. Then it was calcined in a tube heating furnace at 550 °C for 2 h under an Ar atmosphere. After natural cooling, the sample was washed thoroughly before the vacuum freeze-drying process. Then the powder was treated with 0.1M HCl solution for 3 h at ambient temperature for protonation of TiO_{2-x}.

2. Characterization

The crystal structure and morphology of as-prepared samples were analyzed by the X-ray powder diffraction (Lab X XRD-6100, SHIMADZU, a field-emission scanning electron microscopy (JSM-6700F, JEOL) and transmission electron microscopy (JEM-2100Plus, JEOL). Electron spin-resonance spectroscopy (EPR) was operated at a spectrometer (Bruker EPR E500) at room temperature. Chemical compositions of as-prepared products were analyzed by X-ray photoelectron spectroscopy (XPS, Thermo Fisher ESCALAB Xi^+), and the binding energies were calibrated by the C 1s internal standard peak at 284.6 eV. UV-vis diffuse reflectance spectra were performed and recorded on a UV-2600 (SHIMASZU) spectrometer equipped with an integrating sphere attachment (wavelength range 200-800 nm, reference sample: $BaSO_4$). Steady-state photoluminescence spectra were obtained by a time-resolved fluorescence spectrophotometer (Edinburgh Instruments, FLS980) with excitation wavelengths at 325 nm. Nitrogen adsorption/desorption data were obtained with a BET analyzer (BELSORP-Max, MicrotracBEL) and the specific surface area and pore volume were determined using Brunauer-Emmett-Teller (BET) method the Barrett-Joyner-Halenda (BJH) method respectively. The prepared samples were subjected to temperature-programmed desorption (TPD) analysis using a chemisorption device (Autosorb-iQC-

TPX). The transient photocurrent response, Mott-Schottky spectra and impedance spectra were tested using a PMC-1000/DC type one (AMETEK) with a standard three-electrode cell, and a working electrode (FTO film) with a platinum wire counter and Ag/AgCl reference electrode. All the electrochemical measurements used a 1.0 M Na_2SO_4 solution as the electrode. Super-resolution confocal microscope (Leica TCS SP8 STED 3X) was used for collecting fluorescent images. Time of Flight Secondary Ion Mass Spectrometer (ToF-SIMS, M6, ION-TOF) was used to obtain the ToF-SIMS spectrum of IL-TiO_{2-x} to show both PF_6^- and $C_{16}H_{36}P^+$ ions in the negative mode. The contact angle is measured using an optical device called optical contact angle measuring device (DSA100, KRUSS, Germany), which captures images of the liquid droplet or air bubble on the solid surface and calculates the contact angle using image analysis software.

3. Evaluation of photocatalytic activity

All the tests of nitrogen fixation performance were carried out under ambient conditions. A certain amount of IL (0, 10, 20, 30, 40, 50mg) and 10 mg of the as-prepared photocatalysts were dissolved in 15 mL methanol and stirred for 1 h at room temperature before adding 45 mL ultrapure water. Here methanol is not only the sacrificial electron donor but also used to dissolve $[P_{4,4,4,4}][PF_6]$. The system was then irradiated by a 300 W xenon lamp without a filter (HSX-F300, NbetBeiJing) at room temperature (298 K) inside a glass reactor to drive the synthesis of ammonia from N_2 and water. Before the reaction, the solution was purged with high-purity nitrogen for 30 minutes to make the solution saturated with N_2 and remove dissolved O_2 from the reactor. NH_4^+ concentration of the reaction solution was analyzed by Thermo Scientific Dionex ion chromatography (ICS-6000) and calculated by the standard curve. Under constant stirring, the anion of the IL, PF_6^-, was mainly enriched on the surface of protonated TiO_{2-x} through electrostatic interaction because the surface of protonated TiO_{2-x} nanosheets was positively charged. For characterization, the TiO_{2-x} modified with IL was separated by high-speed centrifugation, washed with ethanol and distilled water several times, and then dried at 80 °C for 6 h.

The photocatalytic stability tests of photocatalysts were carried out under the same reaction conditions. After each 4 h reaction, the photocatalyst was washed using ultrapure water several times and dried at 60 °C for 8 h for the next test.

The photocatalytic H_2 production was carried out using a closed system with an outer Pyrex reaction cell (100mL) under the same condition. Gas chromatography was used for the quantification of any produced hydrogen in the reaction system.

The apparent quantum yield (AQY%) of the as-prepared photocatalyst was tested under the same reaction conditions as above, using a 385 nm, 435 nm and 475 nm band-pass filter to obtain monochromatic light. The irradiation area of the photocatalytic reactor cell was about 246 cm^2. The AQY% for NH_4^+ was calculated according to the following formula:

$$\mathrm{AQY}(\%) = \frac{\text{number of reaction electrons}}{\text{number of incident photons}} \times 100\%$$
$$= \frac{3 \times \text{number of evolved ammonia molecules}}{\text{number of incident protons}}$$

4. Computational methods

To investigate the N_2 reduction mechanism on the TiO_{2-x} (101) surface, density functional theory (DFT) calculations are employed using the Perdew–Burke–Ernzerhof (PBE) generalized gradient approximation and the projected augmented wave (PAW) method implemented in the VASP package.[2,3] The electron exchange and correlation potentials were employed by a generalized gradient approximation (LDA+U) with the Perdew-Burke-Ernzerhof exchange–correlation functional in VASP code. The (101) surface supercell of TiO_2 with a lateral size of 10.23 Å × 11.41 Å containing 4 atomic layers was constructed. A vacuum thickness of 15 Å vertical to the slab is adopted to avoid the interaction between two adjacent periodic images. A Monkhorst-Pack K-mesh of 2 × 2×1 was adopted to model the Brillouin zone for the structure optimizations and the vacuum space was 25 Å. The atoms in the two bottom atomic layers are fixed at their bulk positions and other atoms are allowed to relax. Moreover, the long-range vdW interaction was included in the calculations using Grimme-D2 van der Waals

(vdW) correction. The reaction free energy of adsorbed species is obtained via the formula: $\Delta G=\Delta E+\Delta ZPE-T\Delta S$, where ΔE is obtained from the calculated electronic energies, ΔZPE and ΔS are the zero-point energy and entropy change at 298.15 K, respectively. To acquire the free energy profiles, the computational electrode model (CHE) is applied. Structure optimization calculations were done until the total energy changes were within 1×10^{-5} eV per atom and the Hellmann-Feynman force on each atomic site was less than 0.05 eV/Å. All Gibbs free energy values were referenced to the computational hydrogen electrode (CHE) model using the proton-coupled electron transfer (PCET) approach.

In the present work, geometry optimization has been performed on the single-molecule ILs using the Gaussian 09 W program package.[4] The geometry optimization and conformational analysis were performed using the closed-shell hybrid three-parameter exchange-correlation functional Becke-Lee-Yang-Parr (B3LYP) in combination with the 6–311++G(d,p) basis set. [5-7]

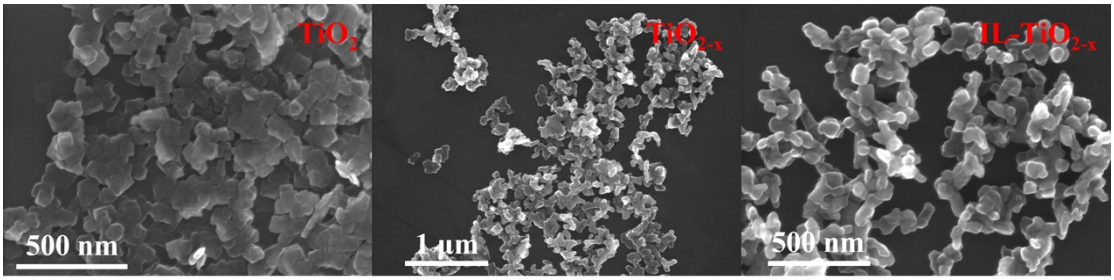

Fig. S1 SEM images of the as-prepared samples.

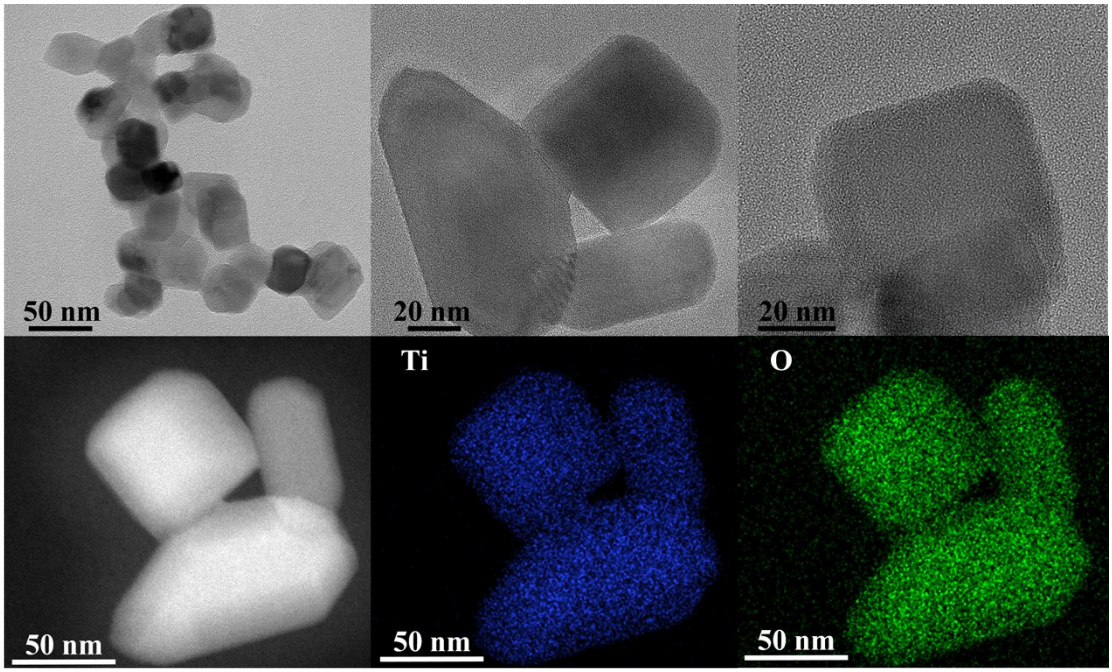

Fig. S2 TEM image and EELS-mapping results of TiO_{2-x}.

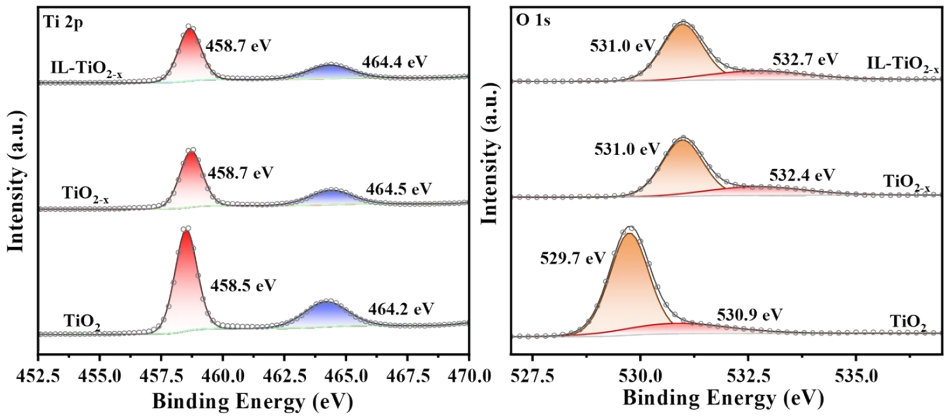

Fig. S3 Ti 2p、O 1s XPS spectra of the as-prepared samples.

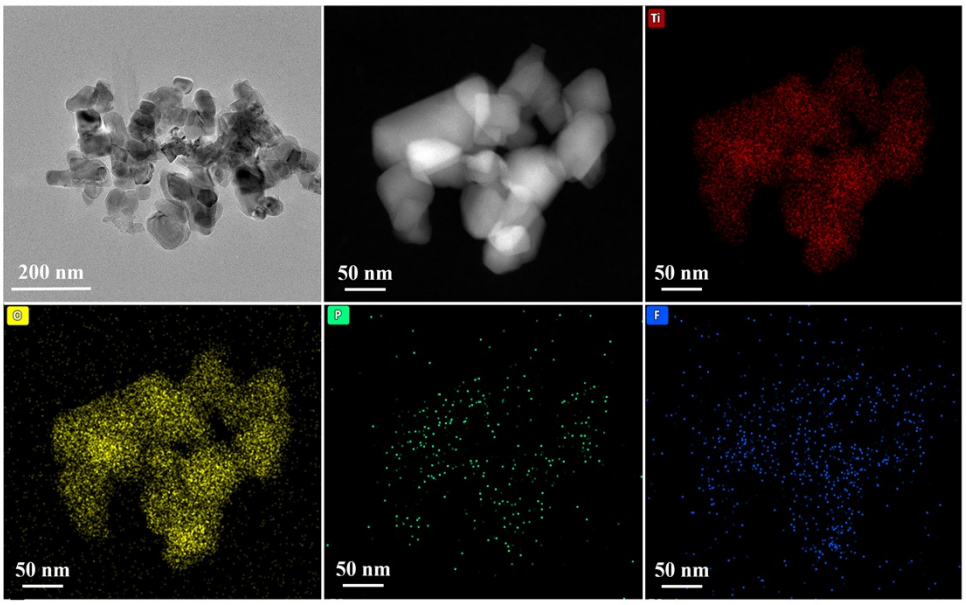

Fig. S4 TEM image and EELS-mapping results of IL-TiO_{2-x}.

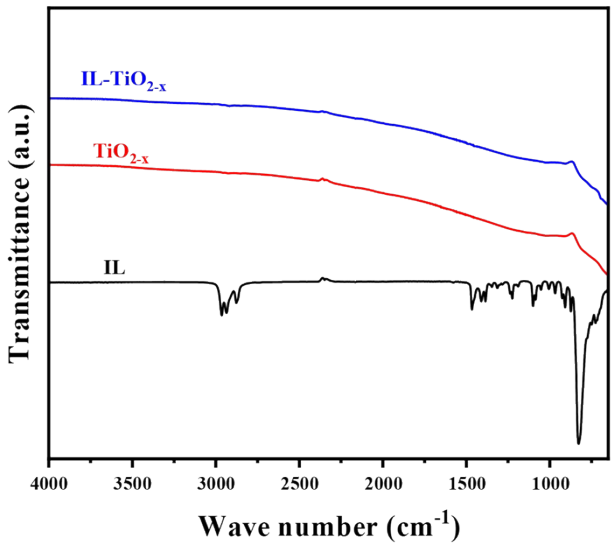

Fig. S5 IR spectra of the as-prepared samples.

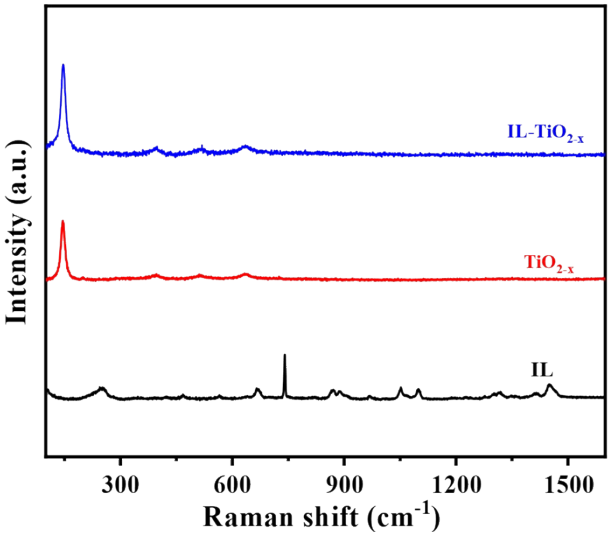

Fig. S6 Raman spectra of the as-prepared samples.

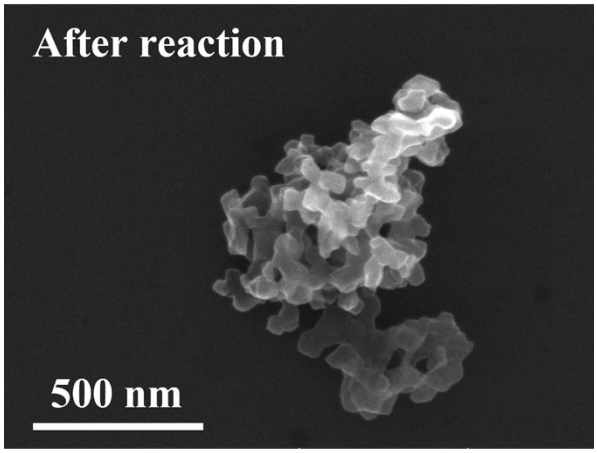

Fig. S7 SEM image of the IL-TiO_{2-x} samples after the cycle runs experiment.

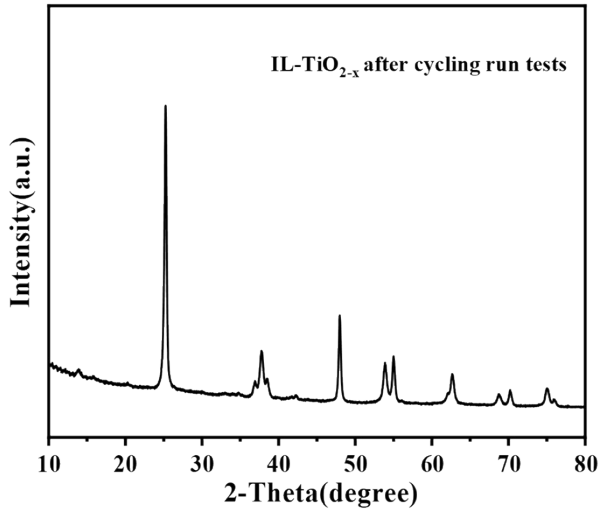

Fig. S8 XRD pattern of the IL-TiO_{2-x} samples after the cycle runs experiment.

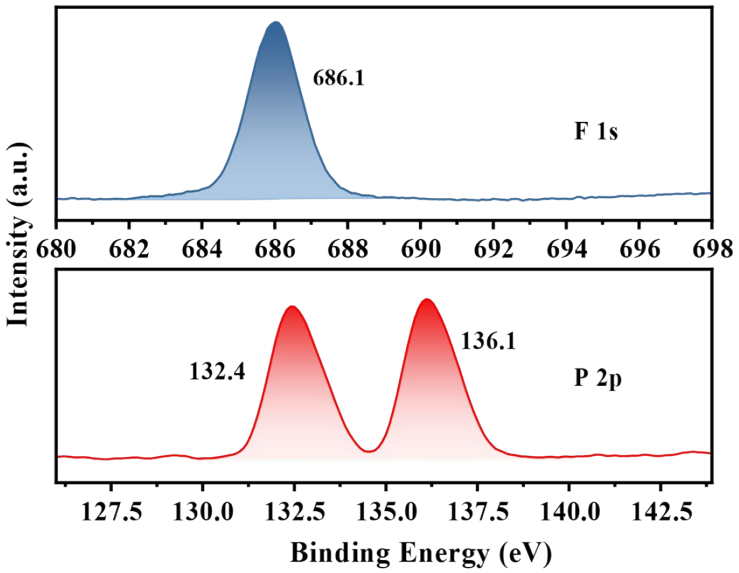

Fig. S9 P 2p and F 1s XPS spectra of the IL-TiO_{2-x} after reaction.

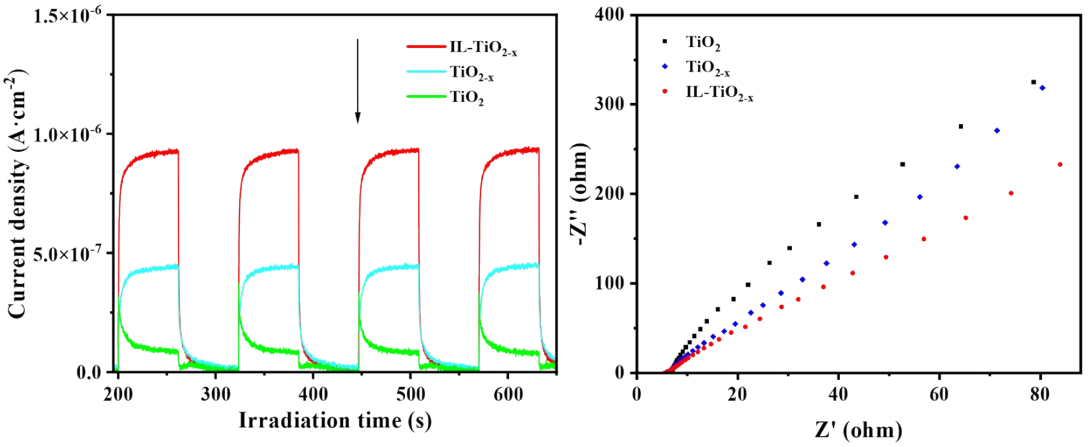

Fig. S10 Transient photocurrent responses and EIS Nyquist plots of the as-prepared samples.

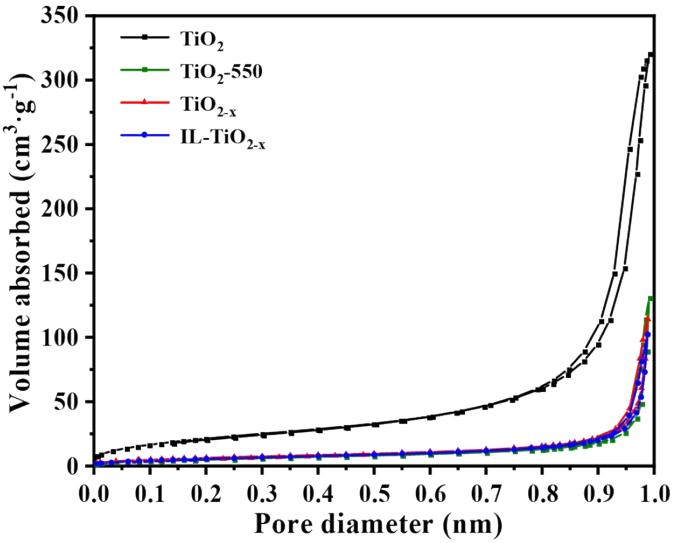

Fig. S11 The N_2 adsorption-desorption isotherms of samples.

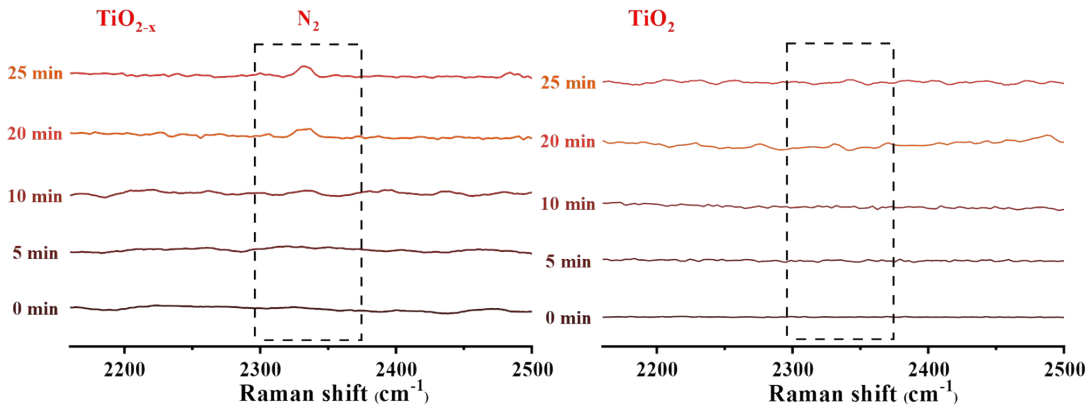

Fig. S12 In situ Raman spectra of TiO_{2-x} and TiO_2 in the nitrogen penetration test.

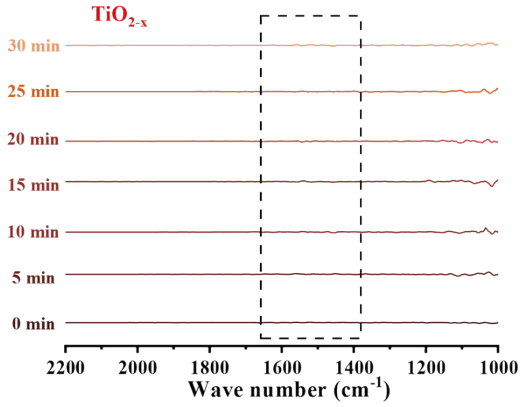

Fig. S13 In situ DRIFT spectra of TiO_{2-x}.

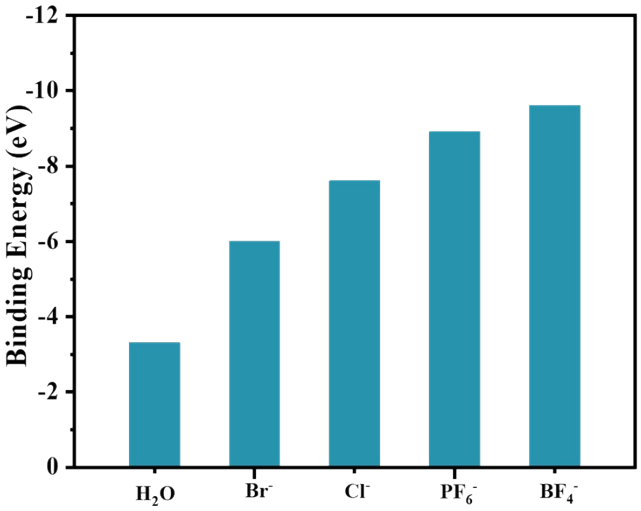

Fig. S14 Binding energy toward N_2 of H_2O and four selected anions calculated with Gaussian.

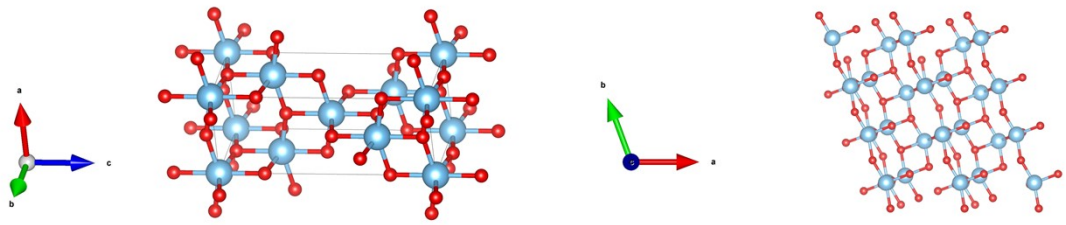

Fig. S15 Corresponding monoclinic perovskite TiO_{2-x} crystal structure and (101) plane structure, blue, and red balls denote Ti and O atoms, respectively.

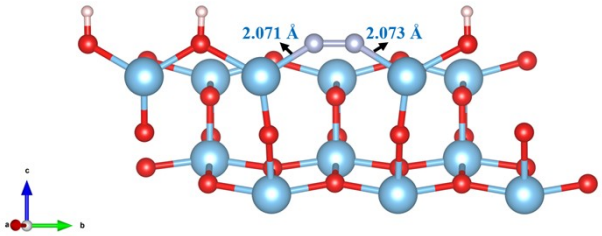

Fig. S16 *N-Ti bond lengths in Å on protonated TiO_{2-x} without PF_6^- involved

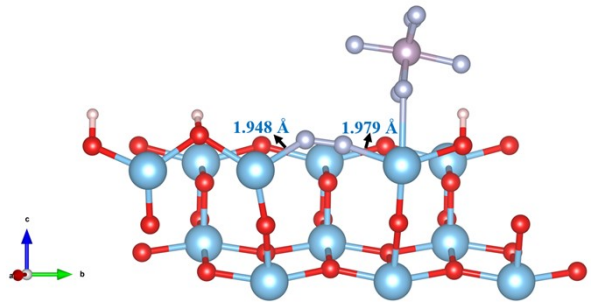

Fig. S17 *N-Ti bond lengths in Å on protonated TiO_{2-x} with PF_6^- involved

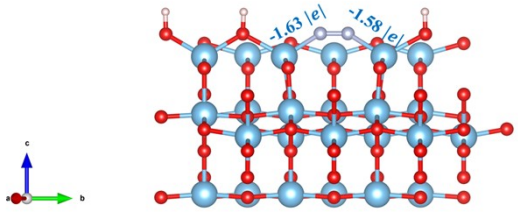

Fig. S18 The adsorption forms of N_2 on protonated TiO_{2-x} without PF_6^- involved and the corresponding Bader charges.

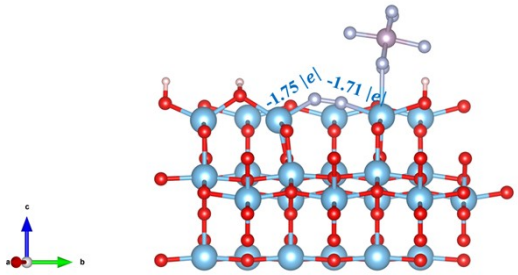

Fig. S19 The adsorption forms of N_2 on protonated TiO_{2-x} with PF_6^- involved and the corresponding Bader charges.

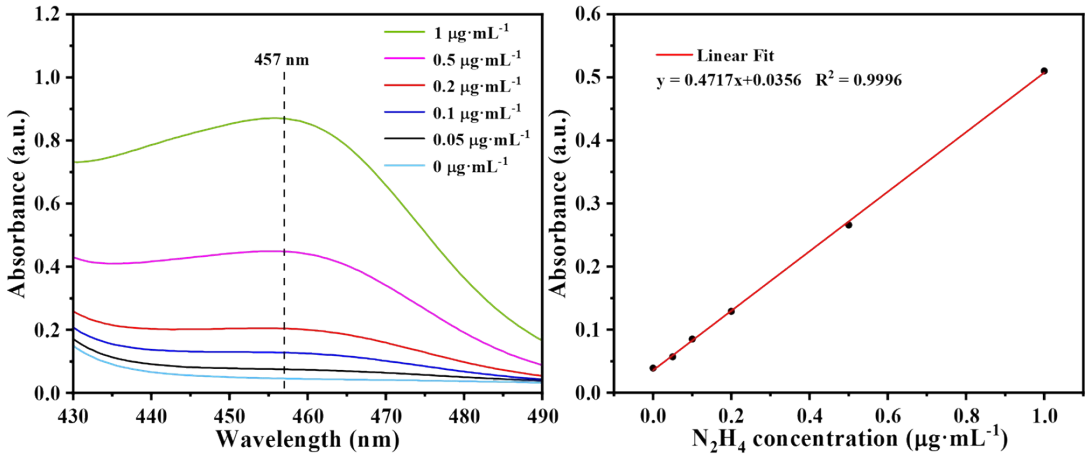

Fig. S20 The UV-vis absorption spectra and the corresponding calibration curve for the colorimetric N_2H_4 assay using the Watt and Chrisp method

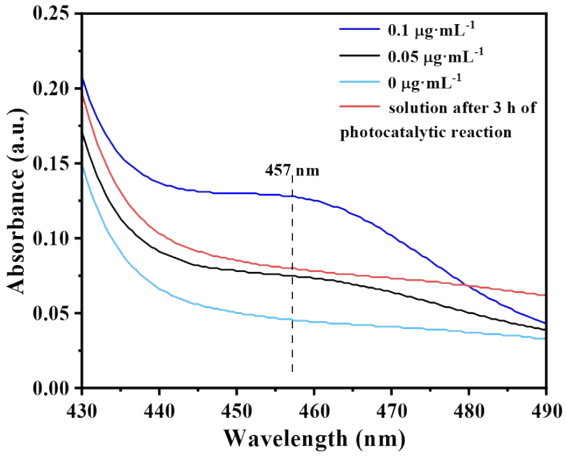

Fig. S21 The concentration of N_2H_4 in the solution after photocatalytic nitrogen fixation of TiO_{2-x} samples tested by the method of Watt and Chrisp

Table S1. The results for photocatalytic N_2 fixation in previous literature about TiO_2 based photocatalysts and our work.

Catalyst	Reaction medium	Scavenger	Ammonia detection method	Ammonia evolution rate (μmol/h·g)	Ref.
TiO_{2-x}	H_2O with IL	methanol	IC	22.7	**This work**
Co-doped TiO_2	H_2O	/	Kruse and Mellon method	6.1	[8]
Fe-doped TiO_2	H_2O	/	Kruse and Mellon method	11.1	[8]
JRC-TiO-6	H_2O	/	IC	3.3	[9]
TiO_2	H_2O	/	Nessler's reagent	6.6	[10]
$AuTiO_2$	H_2O	methanol	The indophenol-blue method	0.8	[11]
TiO_2-OV	H_2O	methanol	The indophenol-blue method	2.2	[11]

Table S2. Concentrations of NH_4^+ and NO_3^- in different solution and the maximum impurity contribution in NH_4^+ yield rate.

No.	NH_4^+ (μmol h^{-1})	NO_3^- (μmol h^{-1})	Maximum impurity contribution in NH_4^+ yield rate (μmol h^{-1})	Experimentally observed NH_4^+ yield rate of TiO_{2-x} (μmol h^{-1})
1	0	0.0081	0.0081	0.50
2	0	0.0085	0.0085	0.53
3	0	0.0083	0.0083	0.50
4	0	0.0079	0.0079	0.61

Table S3. N_2 adsorption-desorption isotherm data analysis of TiO_2, TiO_{2-x} and IL-TiO_{2-x} samples.

sample	SBET (m^2 g^{-1})	Average pore size (nm)	Pore volume (cm^3 g^{-1})
TiO_2	82.8	22.1	0.50
TiO_2-550	21.6	36.5	0.20
TiO_{2-x}	24.5	28.0	0.18
IL-TiO_{2-x}	22.5	27.7	0.16

References

[1] J. Wan, W. Chen, C. Jia, L. Zheng, J. Dong, X. Zheng, Y. Wang, W. Yan, C. Chen, Q. Peng, D. Wang and Y. Li, Adv. Mater., 2018, 11, 1705369.

[2] M. J. Frisch, G. W. Trucks, H. B. Schlegel, G. E. Scuseria, M. A. Robb, J. R. Cheeseman, G. Scalmani, V. Barone, B. Mennucci, G. A. Petersson, H. Nakatsuji, M. Caricato, X. Li, H. P. Hratchian, A. F. Izmaylov, J. Bloino, G. Zheng, J. L. Sonnenberg, M. Hada, M. Ehara, K. Toyota, R. Fukuda, J. Hasegawa, M. Ishida, T. Nakajima, Y. Honda, O. Kitao, H. Nakai, T. Vreven, J. A. Montgomery, Jr., J. E. Peralta, F. Ogliaro, M. Bearpark, J. J. Heyd, E. Brothers, K. N. Kudin, V. N. Staroverov, R. Kobayashi, J. Normand, K. Raghavachari, A. Rendell, J. C. Burant, S. S. Iyengar, J. Tomasi, M. Cossi, N. Rega, J. M. Millam, M. Klene, J. E. Knox, J. B. Cross, V. Bakken, C. Adamo, J. Jaramillo, R. Gomperts, R. E. Stratmann, O. Yazyev, A. J. Austin, R. Cammi, C. Pomelli, J. W. Ochterski, R. L. Martin, K. Morokuma, V. G. Zakrzewski, G. A. Voth, P. Salvador, J. J. Dannenberg, S. Dapprich, A. D. Daniels, Ö. Farkas, J. B. Foresman, J. V. Ortiz, J. Cioslowski and D. J. Fox, Gaussian 09, Revision D.01, Gaussian, Inc., Wallingford CT, 2009, vol. 121, pp. 150–166.

[3] P. J. Stephens, F. Devlin, C. Chabalowski and M. J. Frisch, J. Phys. Chem. B, 1994, 98, 11623–11627.
[4] M. P. Andersson and P. Uvdal, J. Phys. Chem. A, 2005, 109, 2937–2941.
[5] J. P. Merrick, D. Moran and L. Radom, J. Phys. Chem. A, 2007, 111, 11683–11700.
[6] I. M. Alecu, J. Zheng, Y. Zhao and D. G. Truhlar, J. Chem. Theory Comput., 2010, 6, 2872−2887.
[7] M. G. Freire, C. M. S. S. Neves, I. M. Marrucho, J. A. P. Coutinho and A. M. Fernandes, J. Phys. Chem. A, 2010, 114, 3744-3749.
[8] G. N. Schrauzer and T. D. Guth, J. Am. Chem. Soc., 1977, 99, 7189–7193.
[9] H. Hirakawa, M. Hashimoto, Y. Shiraishi and T. Hirai, J. Am. Chem. Soc., 2017, 139, 10929–10936.
[10] J. Li, D. Wang, R. Guan, Y. Zhang, Z. Zhao, H. Zhai, Z. Sun, ACS Sustainable Chem. Eng., 2020, 8, 18258–18265.
[11] J. Yang, Y. Guo, R. Jiang, F. Qin, H. Zhang, W. Lu, J. Wang and J. C. Yu, J. Am. Chem. Soc., 2018, 140, 8497–8508